



Effect of relative humidity on the reaction products of alkali activated fly ash

M. Criado^{a,*}, A. Fernández Jiménez^b, I. Sobrados^c, A. Palomo^b, J. Sanz^c

^a Centro Nacional de Investigaciones Metalúrgicas (CSIC), Avda. Gregorio del Amo 8, 28040 Madrid, Spain

^b Instituto Eduardo Torroja de Ciencias de la Construcción (CSIC), Serrano Galvache 4, 28033 Madrid, Spain

^c Instituto de Ciencia de Materiales de Madrid (CSIC), Sor Juana Inés de la Cruz 3, 28049 Cantoblanco-Madrid, Spain

Abstract

The alkali activation of fly ash (AAFA) is a chemical process in which the ash is mixed with an alkaline activator and cured at a mild temperature to generate compact solids. Both the curing conditions (temperature, time, relative humidity, etc.) and the nature and concentration of the alkali activator play a key role in the development of AAFA micro- and nanostructure, and consequently the properties of these materials. In the present study, fly ash was activated with a 15% water-glass (Na_2SiO_3) + 85% 10-M NaOH solution at 85 °C for 12 h, 7 and 30 days. Two curing methods were used, in which the variable was the relative humidity (RH).

© 2011 Elsevier Ltd. All rights reserved.

Keywords: Fly ash; B. Electron microscopy; B. Spectroscopy; C. Mechanical properties; D. Silicate

1. Introduction

Alkaline cements are the object of growing interest given their potential to enable the industry to operate within CO₂ emissions ceilings. The alkali activation of type F fly ash consists of mixing the ash with highly alkaline solutions (pH > 13) and subsequently curing the resulting paste at a certain temperature to produce a solid material.¹ The main reaction product in the alkali activation of fly ash (AAFA) is an alkaline aluminosilicate hydrate (N–A–S–H) gel. This product contains silicon and aluminium tetrahedra homogeneously distributed in tetrahedral networks. The cavities formed in cross-linked networks of gels accommodate alkaline cations that offset the electrical charge generated when Si^{4+} are replaced by Al^{3+} ions.²

The most prominent parameters in N–A–S–H gel synthesis include the nature of the starting materials, the nature and concentration of the alkali activator and the curing conditions (temperature, time and relative humidity (RH)). The aluminosilicate gel formed depends not only on the concentration of the soluble silica added, but also on its degree of polymerisation, which in turn depends on the alkalinity of the solution.^{5,6}

The apparent structural stability of aluminosilicate gel is known to increase when soluble silica is added to the activating solutions.^{3,4} According to some studies on fly ash,^{5,6} the incorporation of small amounts of soluble silica to the system shortens the time needed for the tectosilicate networks to achieve long-range structural order. The inclusion of silica also expedites the kinetics of the transformation of N–A–S–H gel to zeolites. Moreover, the presence of silicate ions in alkaline solutions raises the silicon content of the aluminosilicate gel, the component responsible for the excellent mechanical properties of these gels.⁷

Previous studies^{8,9} showed that if thermal treatment is prolonged in alkaline media, the hydrothermal reaction may lead to the formation of semi-crystalline or polycrystalline phases. A rise in synthesis temperature, in turn, suffices to raise structural order in synthesised mineral polymers.¹⁰ In addition to curing time and temperature, relative humidity has been shown to play an active role in curing processes of alkali-activated fly ash cements. Unsuitable curing conditions may accelerate carbonation,^{11–13} lowering pH levels and as a result retarding ash activation, with the concomitant water loss and persistence of a high aluminium content in the gels formed. Under these conditions, the final product is granular, porous and characterised by low mechanical strength.

The present study aimed to establish a correlation between the effect of soluble silica in activating solutions and the

* Corresponding author.

E-mail address: mcriado@cenim.csic.es (M. Criado).

Table 1
Chemical composition of the fly ash (wt%) used in the experiments.

	L.I. ^a	I.R. ^b	SiO ₂	Al ₂ O ₃	Fe ₂ O ₃	CaO	MgO	SO ₃	K ₂ O	Na ₂ O	TiO ₂	Total
%	3.59	0.32	53.09	24.80	8.01	2.44	1.94	0.23	3.78	0.73	1.07	100

^a Loss on ignition.

^b Insoluble residue.

relative humidity during curing on the nature and composition of products formed in alkali-activated fly ash reactions. These two parameters induce opposing effects (a small amount of soluble silicate favours reaction kinetics while unsuitable curing conditions retard ash activation). Consequently, the present study was designed to determine which of the two parameters is more relevant.

2. Experimental

The chemical composition of the class-F fly ash supplied by the coal-fired power plant at Compostilla in León, Spain, is given in Table 1. The alkaline solution, containing 15% water-glass + 85% 10-M NaOH (labeled W15, SiO₂/Na₂O = 0.19) was applied to activate the ash. This solution was prepared with (Panreac SA) ACS-ISO 98% sodium hydroxide (NaOH) pellets and waterglass (Na₂SiO₃) with a density of 1.38 g cm⁻³, whose composition was: 8.2% Na₂O, 27% SiO₂ and 64.8% H₂O.

The fly ash was mixed with the activating solution (liquid/solid = 0.4) to prepare the pastes. Immediately after mixing, the pastes were poured into 1 × 1 × 6-cm³ prismatic moulds and cured in an oven at 85 °C for 12 h or 7 or 30 days. The curing conditions were varied to ascertain whether the curing atmosphere affected the mechanical and chemical evolution of the materials. The two methods applied were:

- Method 1, in which moulds containing the paste were placed in air-tight containers that maintained the relative humidity at 90%.
- Method 2, in which moulds were placed directly in the oven alongside a porcelain vial, whereby the relative humidity was ≈40–50%.

The materials were removed from the oven at the specified times and examined with FTIR, MAS-NMR, SEM and BSE/EDS to determine the microstructure and nanostructure of the products formed. FTIR analysis was conducted with KBr pellets containing the samples on an ATI MATTSON GENESIS spectrometer, using a scanning range of 4000–400 cm⁻¹.

²⁹Si and ²⁷Al MAS-NMR (Avance-400 Bruker analyser) studies were conducted on the original ash and alkali-activated pastes formed at different reaction times. The resonance frequencies were 79.5 and 104.3 MHz (*B*₀ = 9.4 T). The spinning rate of the samples in the MAS experiments was 10 kHz. Spectra were recorded using $\pi/2$ (5 μ s) pulses and 5 s intervals between accumulations. All measurements were taken at room temperature with TMS (tetramethylsilane) and Al(H₂O)₆³⁺ as external standards. The error in chemical shift values was estimated to be lower than 0.5 ppm.

The SEM and BSE studies were run on a JEOL JSM 5400 scanning electron microscope fitted with a LINK-ISIS energy dispersive (EDS) analyser (for elemental analysis a total of 15 acquisitions were obtained per sample). The mechanical properties of the 12-h and 7- and 30-day activated ash were determined by testing prismatic specimens to failure on an Ibertest (Autotest-200/10-SW) test frame (12 prisms per series were tested).

3. Results and discussion

The IR spectrum for the original ash (FA spectrum) exhibited two very wide and intense bands characteristic of internal vibrations in TO₄ tetrahedra (T = Al, Si) (see Fig. 1). The band at around 1078 cm⁻¹ (peak 4) was associated with T–O bond asymmetric stretching vibrations, while the other, centred at 460 cm⁻¹ (peak 13), was assigned to internal T–O–T bond bending vibrations.

The presence of quartz in the original ash gave rise in the IR spectrum to a series of bands located at 1150, 1084, 796–778 (double band), 697, 668, 522 and 460 cm⁻¹ (peaks 3, 4, 6, 7, 8, 11 and 13, respectively).¹⁴ The bands at around 1180–1130 cm⁻¹ (peak 3) and 560–550 cm⁻¹ (peak 11, associated with octahedral aluminium) were attributed to mullite.^{15,16}

A more detailed study of the 1400–750 cm⁻¹ region was conducted to analyse the evolution of different phases during alkaline activation and storage at 85 °C for different times. The signals appearing at 996, 1081 and 1185 cm⁻¹ were attributed, respectively, to the vitreous phase of the fly ash, quartz and mullite, while the signal at 1145 cm⁻¹ was generated by the quartz and mullite in the starting materials (see FA spectrum, Fig. 2). The new component appearing at around 1018–998 cm⁻¹ (whose position varied depending on curing method and time) was attributed to the sodium aluminosilicate hydrate gel formed as a result of activation. Constant widths were assumed for all the signals in the spectral deconvolutions shown in Fig. 2. The regression coefficient (*r*²) found ranged from 0.99924 to 0.99194.

The amount of vitreous phase was observed to decline with reaction time in Method 1 specimens, but remained practically constant in the materials obtained with curing Method 2. While the amount of N–A–S–H gel clearly rose in materials cured at high humidity, no significant variations were detected at lower humidity. In the latter specimens, quartz and mullite were scantily affected and the ash dissolved slowly due to the inappropriate curing conditions, retarding the formation of the aluminosilicate gel.

The position of the T–O bond asymmetric stretching band varied depending on relative humidity. In the initial ash it appeared at 1078 cm⁻¹ (peak 4 in Fig. 1), but shifted first towards

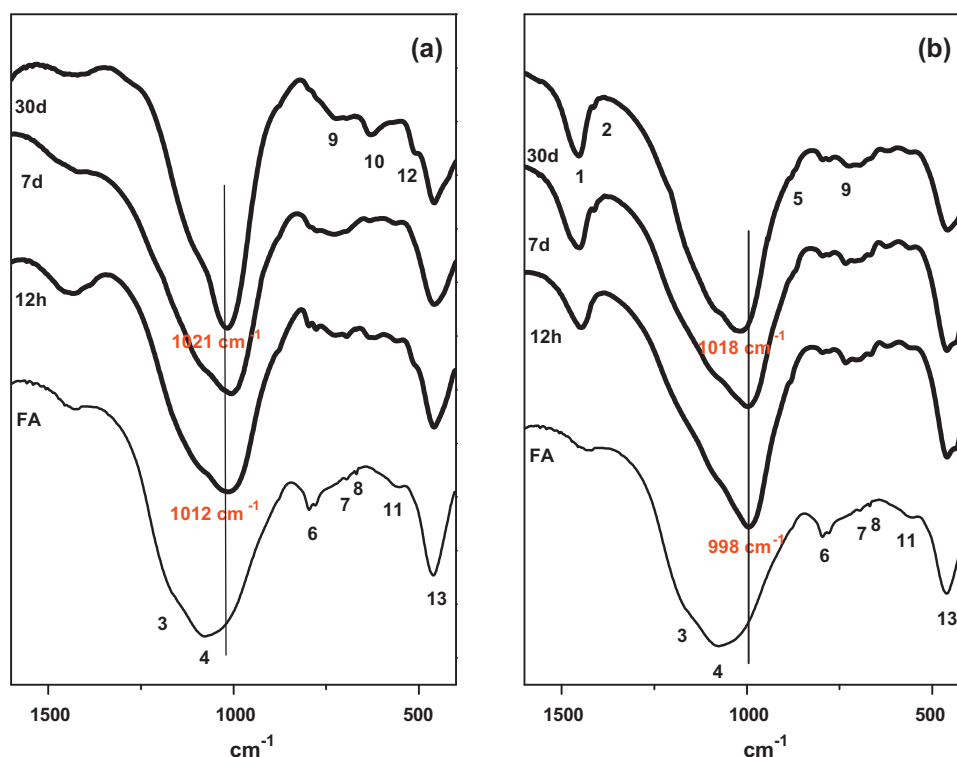


Fig. 1. FTIR spectra for the original ash and the 12-h and 7- and 30-day specimens activated at 85 °C: (a) Method 1 and (b) Method 2.

lower and then back to higher frequencies during activation (Fig. 2). In earlier papers,^{5,17} this pendular movement was associated with the consecutive formation of two gels: the first, an Al-rich gel (Gel 1), that subsequently evolved into a Si-rich gel (Gel 2), improving the mechanical properties of the materials.¹⁸ This band only shifted towards lower frequencies in the pastes cured with Method 2 (50% RH), in which gels with a lower Si/Al ratio were formed (Fig. 2b). In these samples, the band appearing at 460 cm⁻¹ (peak 13, Fig. 1), attributed to the T–O–T bond bending vibrations, remained at the same position during these treatments.

A second important finding was observable in Fig. 1 in connection with the zeolite formation during the activation reaction. The materials cured with Method 1 had a higher zeolite content, consisting of hydrated sodalite (peak 9 in Fig. 1a) and chabazite-Na (peaks 10 and 12 in Fig. 1a). The presence of these zeolites was confirmed with XRD (data not shown). Only hydrated sodalites (peak 9) and alkaline bicarbonates (peaks 1, 2 and 5) were detected in the specimens prepared with Method 2 (Fig. 1b). As a result of the formation of alkaline bicarbonates, the solution pH declined, rendering the alkali reaction less effective and substantially reducing the rate of Si-rich gel formation.

In materials cured at RH ≈40–50%, the degree of carbonation proved to be critical. The fairly scant amount of water also retarded the dissolution of the vitreous fly ash component. These conditions appeared to have a greater effect on silicate than aluminate species, as aluminium dissolves more rapidly than silicon.¹⁷ That would explain the small amounts of sodium aluminosilicate hydrate gel that precipitated at this lower

humidity. This gel was aluminium-rich and its silicon content hardly suffered variations over time.

The amount of silicon taken up in the gels was analysed with ²⁹Si NMR spectroscopy. The ²⁹Si MAS-NMR spectrum of the original vitreous ash (FA) was characterised by a very wide, poorly defined signal, with peaks at –80, –84, –95, –100, –104 and –109 ± 1 ppm, denoting the heterogeneous distribution of silicon¹⁹ (Fig. 3). The peak at –91 ppm was attributed to the Q³(3Al) units in mullite²⁰ while most of the peaks appearing above –109 ppm were assigned to the crystalline quartz (Q⁴(0Al) signals)²¹ present in the fly ash.

Some of the silicon signals (–80, –95 and –100 ppm) disappeared in the 12-h activated (Method 1) pastes (Fig. 3a). However, intense peaks appeared at –89, –93, –99, –104 and –109 ppm that were attributed to Al₄, SiAl₃, Si₂Al₂, Si₃Al and Si₄. These five components of Gel 2 reflect the five possible silicon environments in zeolites.^{21,22}

The 12-h ²⁹Si spectrum for the material cured at low relative humidity (Method 2) contained an intense peak at –88 ppm, along with signals at –100, –105 and –112 ppm. These latter three signals, attributed to the vitreous phase in the starting material, indicated that the starting ash barely reacted with the alkaline solution. The signal at –88 ppm, associated with the presence of Q⁴(4Al) units, denoted the formation of an aluminium-rich reaction product (Gel 1). The area of this signal was greater than in the 12-h spectrum for the Method 1 material. The shape of the spectra barely changed with curing time (30 days): the intensity of the signals at –100 and –105 ppm declined slightly, but the appearance of a signal at –93 ppm

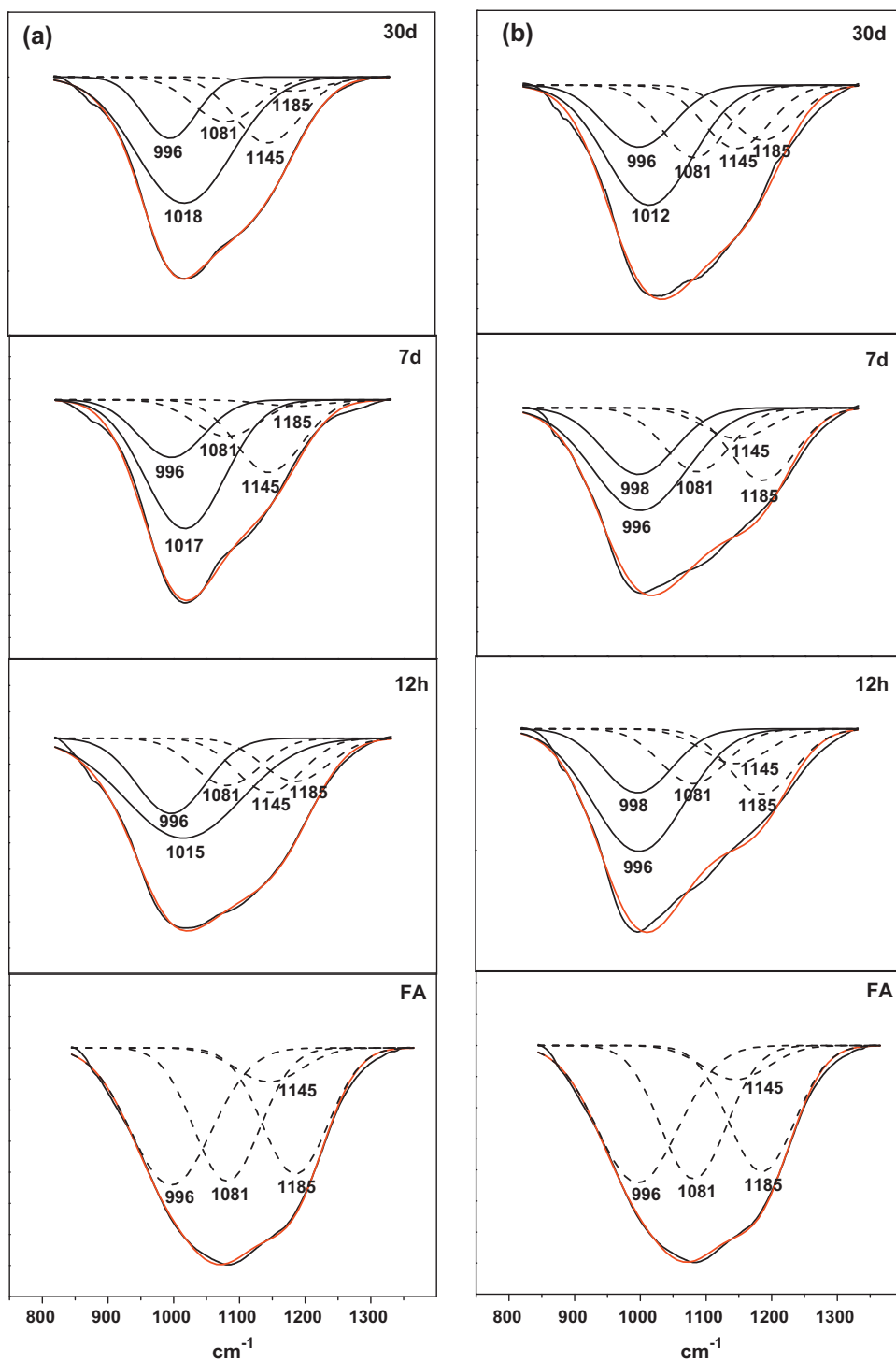


Fig. 2. Deconvolution of the band associated with T–O bond asymmetric stretching vibration in the original ash and in activated 12-h and 7- and 30-day specimens: (a) Method 1 and (b) Method 2.

provided evidence that the fly ash gradually reacted. The resolution of this spectrum was much lower than in the 30-day spectrum for the high relative humidity material obtained with Method 1, an indication that unsuitable curing conditions have a perceptible effect on fly ash activation kinetics.

Fig. 4 shows the components on the ²⁷Al MAS-NMR spectra for the initial ash and reaction products. The ash spectrum contained an intense band at +53 ppm that was assigned to the

tetrahedral aluminium present in the ash. The small band at +1 ppm was attributed to the octahedral aluminium in the mullite present in the fly ash.²⁰

The ²⁷Al MAS NMR spectra for the activated materials exhibited a single component, centred at around +59–60 ppm, that was attributed to the presence of Al(IV) in the reaction products formed. This band had a small broad shoulder at +53.0 ppm generated by the starting ash. According to Mueller et al.²³

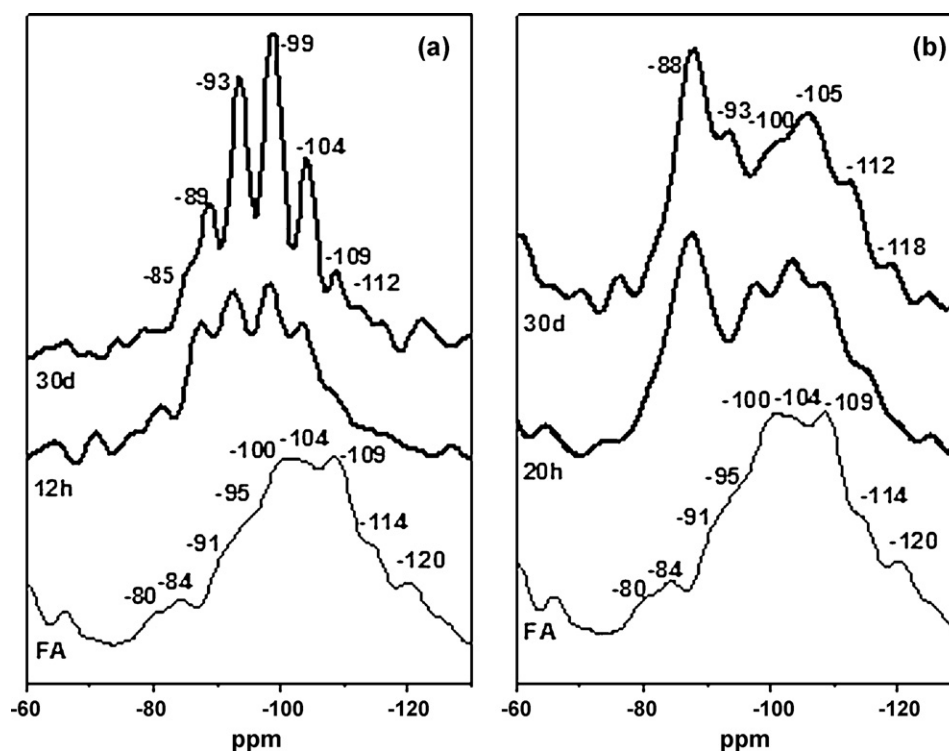


Fig. 3. ^{29}Si MAS NMR spectra for the original and alkali activated ash: (a) Method 1 and (b) Method 2.

and McCormick et al.²⁴, the signal at +59–60 ppm corresponds to $\text{Al}(\text{OSi})_4$ units, i.e., aluminium atoms surrounded by four tetrahedral silicons.

The ^{27}Al MAS-NMR spectra for the activated materials corroborated the FTIR findings, whereby the amount of

vitreous phase declined and the amount of sodium aluminosilicate N–A–S–H gel grew with reaction time (Fig. 2). Method 2 favoured the formation of alkaline bicarbonate (identified with FTIR), lowering the pH and with it the ash activation rate. The outcome was the formation of a smaller amount of N–A–S–H

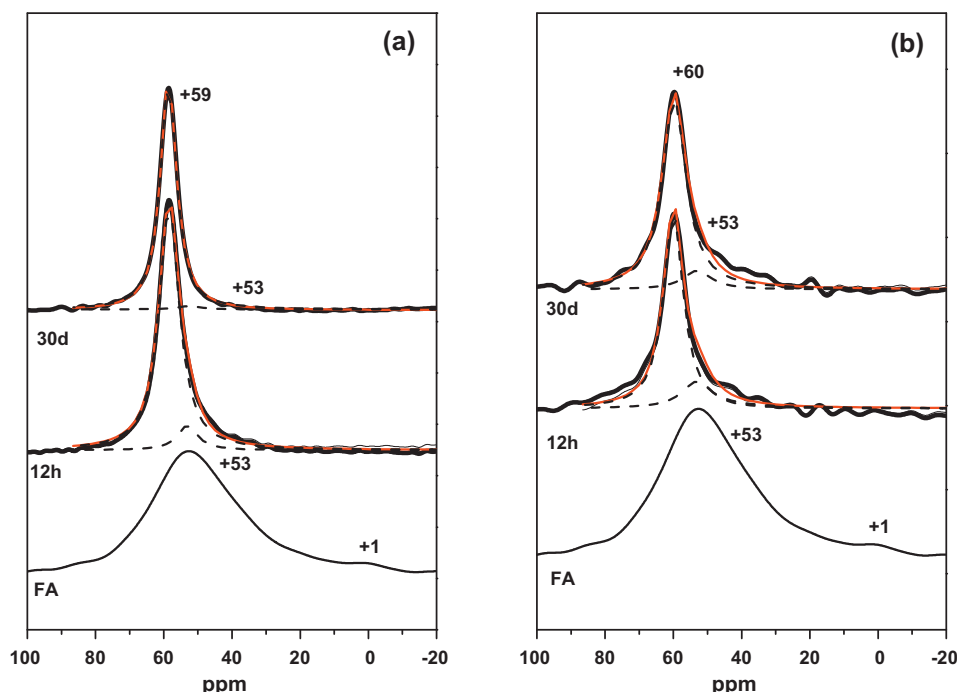


Fig. 4. ^{27}Al MAS NMR spectra for the original and the alkali activated ash: (a) Method 1 and (b) Method 2.

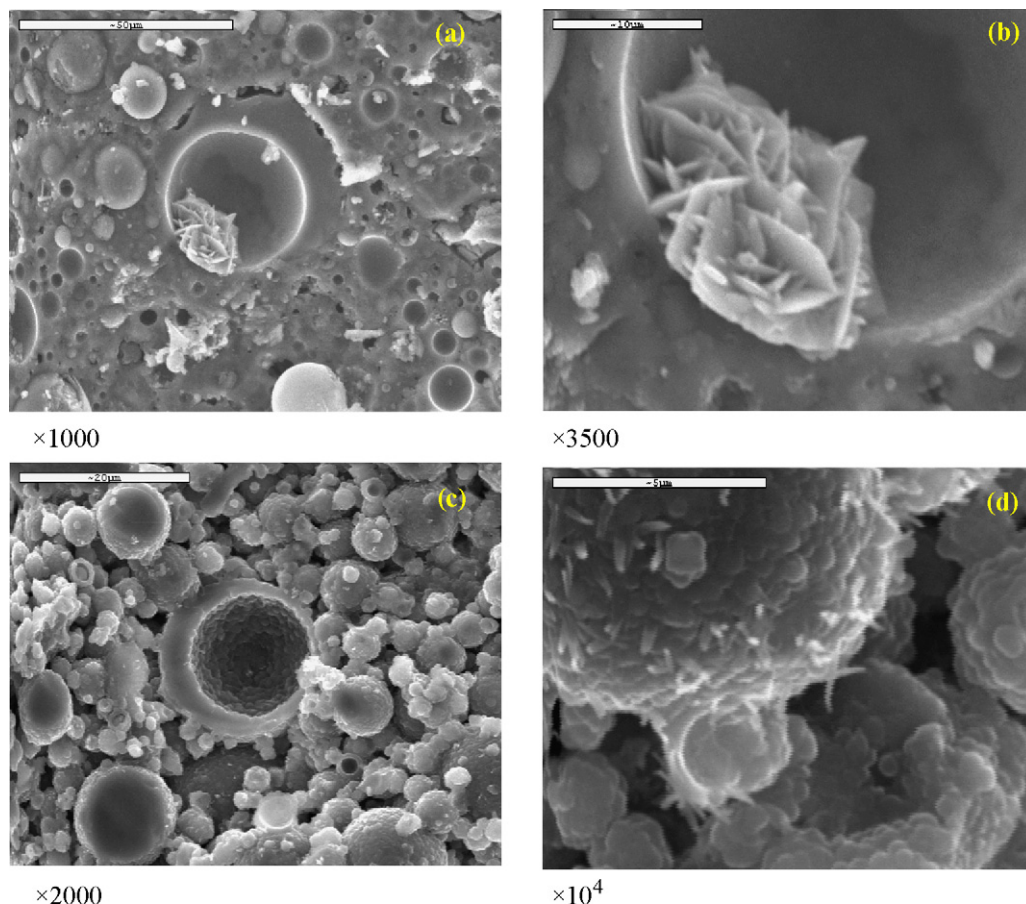


Fig. 5. SEM micrographs of 30-day specimens: (a and b) Method 1 and (c and d) Method 2.

gel than in samples prepared with Method 1 (Fig. 4). The regression coefficient (r^2) obtained for the deconvolutions ranged from 0.99803 to 0.99002.

Fig. 5 shows certain morphological and microstructural characteristics of 30-day, Method 1- and 2-activated ashes. Note the presence of sodium aluminosilicate hydrate, the gel that forms the cementitious matrix, alongside the spheres of unreacted ash.

The matrix in the materials prepared with Method 1 was very compact and contained practically no pores (Fig. 5a). The

reaction product exhibited a surface continuity that resembled a monolayer of abruptly frozen viscous fluid (such as glass), which contrasted sharply with the group of randomly precipitating individual particles visible in the Method 2 material (Fig. 5c). The presence of the alkaline bicarbonates detected in the latter system (Fig. 5d) induced the development of a “granular” morphology in which the ash particles were partially attacked but conserved their initial spherical geometry. Moreover, no zeolites were observed in these matrices. By contrast, the formation

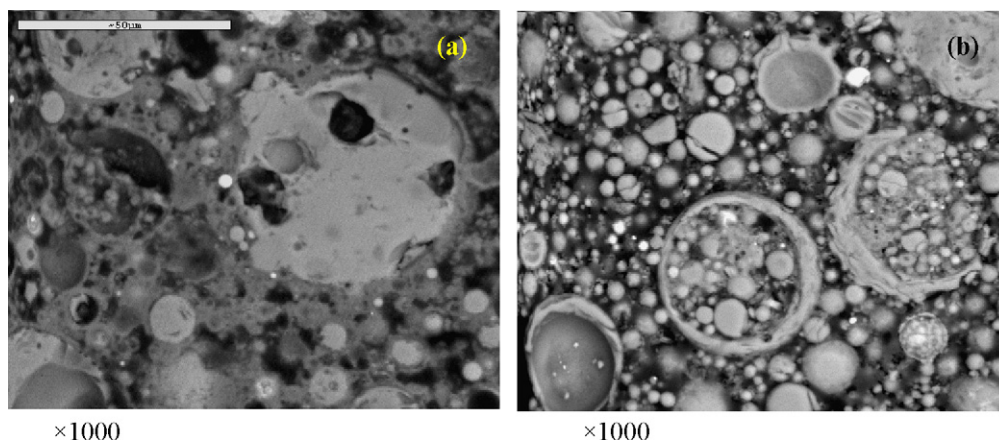


Fig. 6. BSE micrographs of 30-day alkali-activated ash: (a) Method 1 and (b) Method 2.

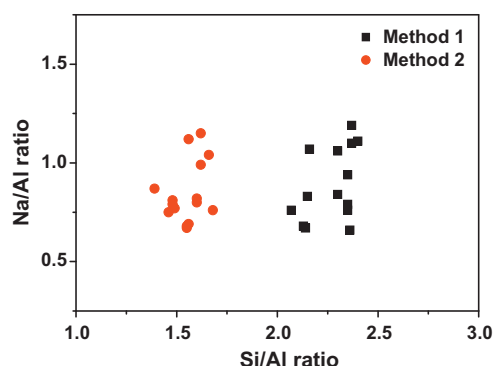


Fig. 7. EDS analysis of 30-day alkali-activated ash: (a) Method 1 and (b) Method 2.

of small zeolite crystals was detected in the Method 1 material (Fig. 5b).

The 30-day microstructures were also studied by BSE, whose results are depicted in Fig. 6. In the images for both systems, the N–A–S–H gel is the darker phase and the fly ash the lighter. The micrograph of the Method 1 specimen (Fig. 6a) showed fly ash particles that were firmly embedded in and connected to the matrix. The BSE image of the Method 2 gels in Fig. 6b, by contrast, showed smaller amounts of N–A–S–H gel and spherical fly ash particles, most of which appeared to be undissolved.

The Si/Al and Na/Al ratios of N–A–S–H gels were determined by EDS analysis (15 analyses per sample). The findings are shown in Fig. 7, where two groups of points can be clearly observed. The N–A–S–H gel formed under low relative humidity conditions had a lower Si/Al ratio than the Method 1 material. Based on the EDS analysis (Fig. 7), the average Si/Al and Na/Al ratios for the Method 1 specimens were 2.27 ± 0.11 and 0.82 ± 0.16 , respectively, and 1.56 ± 0.08 and 0.88 ± 0.19 , respectively, for the Method 2 specimens. When the activating solution contained both Na^+ and soluble Si^{4+} , these two elements were taken up into the reaction products. These ratios were clearly higher than those reported for other activators.¹³ Curing treatments at $\approx 50\%$ RH induced the formation of alkaline bicarbonate in the reaction products (Fig. 5d). The resulting acidification of the medium led to the dissolution of relatively small amounts of Si from the fly ash and consequently a low Si/Al ratio in the main reaction product.

The specimens cured at a higher relative humidity developed higher strength than the samples cured at lower humidity (Fig. 8). Mechanical strength rose visibly with curing time in the Method 1 specimens, but remained essentially flat in the Method 2 pastes. By lowering pH, carbonation had an adverse effect on reaction kinetics and therefore on the development of mechanical strength.

The results of this study concur with earlier findings, where NaOH was used as activator.^{11–13} Curing treatments of alkali activated fly ash cements with a sodium silicate solution (W15, $\text{SiO}_2/\text{Na}_2\text{O} = 0.19$) and relative humidity of around 50% favoured carbonate formation (FTIR and SEM findings). The presence of carbonates, which acidified the medium, together with a paucity of water, rendered activation less effective and reduced both the dissolution rate of the ash (higher percentage

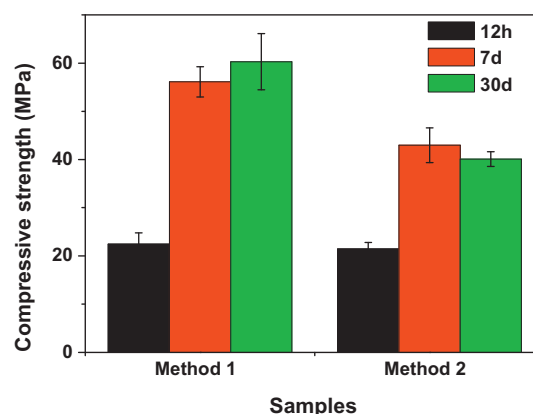


Fig. 8. Specimen mechanical strength vs. curing time for the two systems studied.

of vitreous phase) and the formation rate of the alkaline aluminosilicate hydrate gels (FTIR and NMR findings). The aluminium-rich N–A–S–H gel (Gel 1) forming at low relative humidity had a lower Si/Al ratio than the silicon-rich gel (Gel 2) and a stable composition that remained essentially unchanged over time. Moreover, its granular and porous morphology hampered mechanical strength development.

Nonetheless, a comparison of these results to the findings obtained in prior studies using an 8-M solution of NaOH as the activator revealed that the presence of a small amount of soluble silica in the medium substantially mitigates the adverse effect of unsuitable curing conditions on mechanical strength. Fig. 9 shows the percentage loss of compressive strength in Method 2 with respect to Method 1 for the two alkaline activators (the data for the 8-M NaOH-activated fly ash were drawn from Ref.¹³).

In the absence of soluble silica, the mechanical strength obtained with Method 2 was up to 60% lower than the Method 1 value. In the presence of soluble silica, the difference in strength was perceptibly smaller, ranging from 30 to 40% (see Fig. 9).

The carbonation and concomitant decline in pH that took place in Method 2 must be assumed to have been non-instantaneous, as Fig. 9 shows. Unsatisfactory curing primarily affects mechanical strength at older ages: at early ages the effect is minor. Furthermore, prior studies^{11,12} showed that the presence of a small amount of soluble silica in the medium expedited

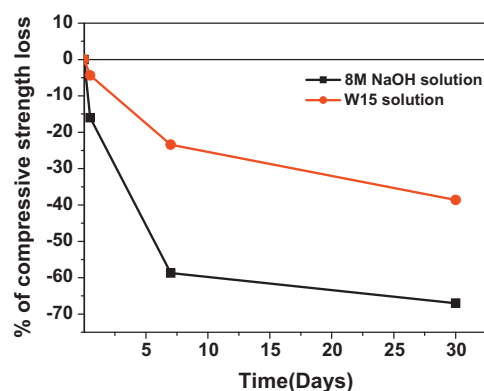


Fig. 9. Percentage loss of compressive strength in Method 2 compared to Method 1 [$\% = ((\text{Strn M1} - \text{Strn M2})/\text{Strn M1}) \times 100$].

the precipitation of N–A–S–H gel, the component primarily responsible for the mechanical properties of these cements. That would explain why, in the presence of soluble silica, deficient curing would affect early (12-h) age pastes only mildly.

The decline in pH in the material cured using Method 2 would hinder silicon dissolution at more mature ages, adversely impacting the ongoing development of mechanical strength. Here also, the effect was less significant when soluble silica was present in the activator, for it favoured ionic species polymerisation, offsetting the effect of carbonation. Prior studies showed that the degree of reaction in the 30-day 8-M NaOH-activated system cured using Method 2 was 41.77%,¹² whereas the value for the system with soluble silica was 44.18%.

The presence of soluble silica also affected material microstructure. Scanning electron microscope studies revealed that the morphology of W15-activated fly ash, even when cured using Method 2, was more compact than the morphology observed when NaOH was the activator.¹³ The samples cured at low relative humidity (Method 2) in the absence of soluble silica developed a scantily compacted structure with substantial numbers of large pores (10–50 μm).¹² One possible explanation for the development of this morphology is that the water may have evaporated completely from the pores during curing. Nonetheless, as noted earlier, the presence of silicate ions in the reaction system furthered species condensation and subsequently stimulated sodium aluminosilicate hydrate polymerisation.

In another vein, although Method 2 did not favour the formation of Si-rich gels, the gels forming in that method in the presence of soluble silica had higher Si/Al ratios than the gels forming under the same curing conditions when NaOH was the activator. In the present study, the 30-day gel formed with solution W15 had an Si/Al ratio of 1.54 ± 0.12 and an Na/Al ratio of 1.03 ± 0.14 . These values were slightly higher than found for the gel of the same age generated in the system activated with caustic soda, where Si/Al and Na/Al were 1.40 and 1.00, respectively.¹³

Based on these findings, relative humidity during initial curing may be concluded to play a crucial role in reaction product composition and structure, as well as in the degree of reaction and the mechanical development of the material. RH has a substantial effect in the presence as well as in the absence of soluble silica. Further to the present study, however, in the presence of soluble silica that effect would appear to be mitigated somewhat, particularly at early ages. In view of the foregoing, both relative humidity and soluble silica may influence system durability in acidic and sulphate environments, as well as other aggressive media such as seawater. An assessment of their respective impact would be an interesting subject for future study.

4. Conclusions

Relative humidity during initial curing plays a highly relevant role in the alkaline activation of fly ash, irrespective of the activator used.

RH values of ≈ 40 –50% favour the formation of alkaline bicarbonates and the loss of system moisture. This decline in pH induced by carbonation and the paucity of water retard the

dissolution of the vitreous component in the fly ash, with an adverse effect on reaction kinetics.

The presence of soluble silica in the activating solution renders the delay in fly ash activation kinetics less pronounced. The soluble Na^+ and Si^{4+} present in the activating solution are taken up into the reaction products. The Si/Al and Na/Al ratios are higher under these conditions than when NaOH is the activator used. Moreover, the addition of waterglass enhances ionic species polymerisation in the system. The waterglass-activated material cured with Method 2 is more compact and its mechanical strength values higher than obtained for NaOH-activated fly ash of the same age cured at the same relative humidity.

Acknowledgements

This research project was funded under Spanish Ministry of Science and Innovation project BIA2010-17530. M. Criado participated in this study under a Post-graduate Studies Council grant (ref. JAE-Doc2007) co-financed by the European Social Fund.

References

1. Palomo A, Gtutzek MW, Blanco MT. Alkali-activated fly ashes: a cement for the future. *Cement Concrete Res* 1999;**29**:1323–9.
2. Palomo A, Alonso S, Fernández-Jiménez A, Sobrados I, Sanz J. Alkaline activation of fly ashes. A NMR study of the reaction products. *J Am Ceram Soc* 2004;**87**:1141–5.
3. Duxson P, Fernández-Jiménez A, Provis JL, Lukey GC, Palomo A, van Deventer JSJ. Geopolymer technology: the current state of the art. *J Mater Sci* 2007;**42**:2917–33.
4. Lee WKW, Van Deventer JSJ. Structural reorganisation of class F fly ash in alkaline silicate solutions. *Colloids Surf A* 2002;**211**:49–66.
5. Criado M, Fernández-Jiménez A, Palomo A. Alkali activation of fly ash. Effect of the $\text{SiO}_2/\text{Na}_2\text{O}$ ratio. Part I. FTIR study. *Micropor Mesopor Mater* 2007;**106**:180–91.
6. Criado M, Fernández-Jiménez A, Palomo A, Sobrados I, Sanz J. Effect of the $\text{SiO}_2/\text{Na}_2\text{O}$ ratio on the alkali activation of fly ash. Part II. ^{29}Si MAS-NMR survey. *Micropor Mesopor Mater* 2008;**109**:525–34.
7. Fernández-Jiménez A, Palomo A. Composition and microstructure of alkali activated fly ash binder: effect of the activator. *Cement Concrete Res* 2005;**35**:1984–92.
8. Rowles M, O'Connor B. Chemical optimisation of the compressive strength of aluminosilicate geopolymers synthesised by sodium silicate activation of metakaolin. *J Mater Chem* 2003;**13**:1161–5.
9. Van Jaarsveld JGJ, van Deventer JSJ. The effect of metal contaminants on the formation and properties of waste-based geopolymers. *Cement Concrete Res* 1999;**29**:1189–200.
10. Barrer RM, White EAD. The hydrothermal chemistry of silicates. Part II. Synthetic crystalline sodium aluminosilicates. *J Chem Soc* 1952;**286**:1561–71.
11. Criado M, Palomo A, Fernández-Jiménez A. Alkali activation of fly ashes. Part I. Effect of curing conditions on the carbonation of the reaction products. *Fuel* 2005;**84**:2048–54.
12. Kovalchuk G, Fernández-Jiménez A, Palomo A. Alkali-activated fly ash: effect of thermal curing conditions on mechanical and microstructural development-Part II. *Fuel* 2007;**86**:315–22.
13. Criado M, Fernández-Jiménez A, Palomo A. Alkali activation of fly ashes. Part III. Effect of curing conditions on reaction and its graphical description. *Fuel* 2010;**89**:3185–92.
14. Gadsden JA. *Infrared spectra of minerals and related inorganic compounds*. London: Butterworths; 1975.

15. Jin X-H, Gao L, Guo JKJ. The structural change of diphasic mullite gel studied by XRD and IR spectrum analysis. *J Eur Ceram Soc* 2002;**22**:1307–11.
16. Temuujin J, Okada K, Mackenzie KJD. Effect of mechanomechemical treatment on the crystallization behaviour of diphasic mullite gel. *Ceram Int* 1999;**25**:85–90.
17. Fernández-Jiménez A, Palomo A. Mid-infrared spectroscopic studies of alkali-activated fly ash structure. *Micropor Mesopor Mater* 2005;**86**:207–14.
18. Fernández-Jiménez A, Palomo A, Sobrados I, Sanz J. The role played by the reactive alumina content in the alkaline activation of fly ashes. *Micropor Mesopor Mater* 2006;**91**:111–9.
19. Fernández-Jiménez A, Palomo A. Characterisation of fly ashes. Potential reactivity as alkaline cements. *Fuel* 2003;**82**:2259–65.
20. He H, Guo J, Zhu J, Yuan P. ^{29}Si and ^{27}Al MAS NMR spectra of mullites from different kaolinites. *Spectrochim Acta A* 2004;**60**:1061–4.
21. Engelhardt G, Michel D. *High resolution solid state NMR of silicates and zeolite*. London: Wiley; 1987.
22. Klinowski J. Nuclear magnetic resonance studies of zeolites. *Prog NMR Spectrosc* 1984;**16**:237–309.
23. Mueller D, Hoebbel D, Gessner W. ^{27}Al NMR studies of aluminosilicate solutions. Influences of the second coordination sphere on the shielding of aluminium. *Chem Phys Lett* 1981;**84**:25–9.
24. McCormick AV, Bell AT, Radke CJ. Multinuclear NMR investigation of the formation of aluminosilicate anions. *J Phys Chem* 1989;**93**:1741–4.